A New Look at Modeling Surface Heterogeneity: Extending its Influence in the Vertical

Andrea Molod *
Department of Earth and Planetary Sciences
The Johns Hopkins University, Baltimore, MD 21218

Haydee Salmun
Department of Geography
Hunter College of the City University of New York, New York, NY 10021

Darryn W. Waugh
Department of Earth and Planetary Sciences
The Johns Hopkins University, Baltimore, MD 21218

June 11, 2002

* Also: Data Assimilation Office, Goddard Space Flight Center, Greenbelt, MD 20771
Corresponding author address: molod@rua.eps.jhu.edu

Abstract

Heterogeneities in the land surface exist on a wide range of spatial scales and make the coupling between the land surface and the overlying boundary layer complex. In this study we investigate the vertical extent to which the surface heterogeneities affect the boundary layer turbulence. We present a technique called 'extended mosaic' which models the coupling between the heterogeneous land surface and the atmosphere by allowing the impact of the subgrid scale variability to extend throughout the vertical extent of the planetary boundary layer. Simulations with extended mosaic show that there is a GCM level at which the distinct character of the turbulence over different land scene types is homogenized, which we call the model blending height. The behavior of the model blending height is an indicator of the mechanism by which the surface heterogeneities extend their direct influence upwards into the boundary layer, and exert their influence on the climate system. Results are presented which show the behavior of the model blending height and the relationships to atmospheric and surface conditions. The model blending height is generally one third to one half of the planetary boundary layer height, although the exact ratio varies with local and climatological conditions and the distribution of the underlying vegetation. The model blending height also increases with canopy temperature and sensible heat flux, and is influenced by the amount of variability in the surface vegetation and the presence of deciduous trees.

1 Introduction

In order to understand and predict the behavior of the earth's climate system it is important to understand how energy, water, carbon and nitrogen are exchanged between the atmosphere and the terrestrial biosphere. The global environment is sensitive to these exchanges at the land surface in part because over 70% of the energy absorbed into the climate system is absorbed at the Earth's surface, and one third of the surface is land. The land surface interacts with the global environment in part due to the creation and dispersion of aerosols, the surface radiation which is governed by the surface albedo and emissivity, and the variations in surface roughness and surface hydrology. The effects of these interactions may extend beyond the regions in which they are initiated by inducing modifications of the large scale circulation. For example, because the tropics are the primary energy source and the major moisture source for the global climate, changes in the land surface in the tropics may influence the tropical jets and global climate (Dickinson and Kennedy 1992; Polcher and Laval 1994; Henderson-Sellers et al. 1993).

The character of the land surface is highly variable, as has been shown clearly by LANDSAT and other visible imagery (DeFries et al. 2000). The heterogeneity of the land surface exists over a wide range of spatial scales which are determined by the variability of vegetation cover, the types of terrain, soil texture and wetness, the amount of cloud cover and the extent of urban areas. These heterogeneities will determine in part the impact on climate of land use change such as deforestation, urbanization and desertification. The scale of these heterogeneities may be smaller, and in some cases much more so, than the characteristic grid scale in most current General Circulation Models (GCMs) used in climate studies. The influence of surface heterogeneities is felt by the atmosphere up to some level, generally above the surface layer and within the planetary boundary layer, as indicated by observational and modeling studies (Claussen 1995; Mahrt 2000 and papers cited therein). These studies deal mainly with the concept of the blending height as the level at which the flow over patchy terrain is homogenized. The present study is aimed at understanding the implications of the vertical extent of the influence of surface heterogeneities for a GCM's description of the coupling at the earth- atmosphere interface.

In general, the effects of heterogeneities on scales smaller than the typical grid scale in global climate models are difficult to model. The effects of these heterogeneities can be characterized as 'aggregation' effects and 'dynamical' effects, the first arising directly from spatial heterogeneity in the land surface and the second associated with the small scale (micro and mesoscale) circulations induced by heterogeneous surfaces (Georgi and Avissar 1997). Both effects of heterogeneity are important in modeling land surface processes and interactions within climate models, but it is the aggregation effects that are captured in almost all present day GCMs. Existing techniques to capture these effects include 'composite' which accounts for the subgrid-scale variability by specifying soil and vegetation parameters that represent a homogeneous 'composite' vegetated surface, and 'mosaic' which calculates separate heat and moisture balance equations for each vegetation type contained within a GCM grid square. The conceptualization of each GCM grid square as having homogeneous, albeit composite vegetation and soil characteristics does not allow for the direct propagation of the independent characteristics of each vegetation type into the atmosphere at all. Mosaic does not account for the vertical influence of the land surface heterogeneities beyond the height of the surface layer, even though the blending height scaling arguments summarized in Mahrt (2000) suggest that the effects of the heterogeneities are felt well into the planetary boundary layer. This may well constitute an important limitation to capturing the effectiveness of the communication between the land surface heterogeneity and the atmosphere (Mahrt 2000).

This restriction may be overcome in a GCM parameterization of the land-atmosphere coupling which allows for an extended vertical influence of surface heterogeneities, given sufficient GCM vertical resolution in the boundary layer. This paper presents a technique called 'extended mosaic' which models the coupling between the heterogeneous land surface and the atmosphere by allowing the impact of the subgrid scale variability to extend throughout the vertical extent of the planetary boundary layer. In the next section we briefly review the concept of the blending height and its scaling, as well as the implications of this scaling for a GCM scheme. The extended mosaic technique is described in section 3, followed by a section defining a 'model blending height' (MBH). In section 5 we present and examine the variability of the MBH and the relationship with other atmospheric quantities using a GCM simulation with extended mosaic, and the study is summarized in the final section.

2 The Blending Height

Early studies of the vertical influence of the land surface heterogeneities were conducted by Wieringa (1986), where he defined the blending height as the level inside the planetary boundary layer above which the flow becomes horizontally homogeneous in the absence of other influences. Many studies using field measurements have determined that, under neutral conditions, where the spatial inhomogeneities are described by variations in roughness alone, the blending height is variable, depends mostly on the nature of the surface roughness elements, and ranges from 20 to 100 times the size of the local roughness length (Garrat 1980; Parlange and Katul 1995; Himaya et al. 1996; Brutsaert 1998; and others). These studies were limited to small horizontal scales (less than 10 km). Mason (1988) extended the analysis to include larger horizontal scales, and characterized a relationship between the horizontal scale of the variability L_h and the blending height l_b. This scaling relationship is based on the assumption that the boundary layer flow is mainly determined by a balance between vertical advection and the divergence of the vertical turbulent flux. Claussen (1995) determined that from Mason's heuristic model one can conclude that $l_b \sim 0.01 \times L_h$. This estimate agrees with the blending height estimates reported by the early studies, where a horizontal scale of 10 km would imply a blending height of 100 m. For horizontal scales of heterogeneity of the order of 50 to 100 km or larger that characterize part of the globe, this would imply a blending height of 500 m to 1 km. A comprehensive survey of different blending height estimates under different atmospheric conditions was presented by Mahrt (1996), where he reported that l_b can be as high as the height of the planetary boundary layer, or even higher for an unstable atmosphere under the influence of strong surface heating. A typical scaling relationship is of the form: $l_b = C_c(w^*/U)L_h$, where w^* is a convective vertical velocity scale, U is a scale for the mean horizontal wind, and C_c is a constant (Raupach and Finnegan 1995).

In analogy to this discussion of blending heights, it is possible to construct a conceptual model of the blending process for the larger scales resolved by climate models. In this conceptual model, the mosaic aggregation technique, which aggregates the turbulent fluxes out of the surface layer, can be viewed as setting the blending height of the model at the surface layer. The extension of the concept of a blending height to larger scales was briefly mentioned in Bringfelt et al. (1999), where they explicitly state that mosaic assumes that the blending height is at the surface layer, and that this might not be an adequate representation of the impact of surface heterogeneity. The recognition that mosaic cannot account for the extended vertical influence of the land surface variability was noted earlier by Koster and Suarez (1992b). The limitations of mosaic in this regard was suggested by the results of a study by Mölders et al. (1996). They compared mosaic to an explicit subgrid scale model, and reported that the differences are small in the middle to upper troposphere and that these differences increase with proximity to the surface starting inside the atmospheric boundary layer. The extended mosaic technique, presented in the next section, attempts to address these limitations of mosaic discussed here.

3 The 'Extended Mosaic' Technique

'Extended mosaic' (EM) is a new technique which follows the mosaic approach and extends the direct influence of surface heterogeneities upwards throughout the entire depth of the turbulent atmospheric boundary layer. EM is the technique used to couple the land surface model to the turbulent atmospheric boundary layer. The essence of this technique is the interplay between processes that occur in grid space and processes that occur in tile space, and the extension of that interplay throughout the depth of the turbulent layer. EM was originally developed for use in the GEOS-Terra GCM (Molod 1999), which includes a parameterization of turbulent fluxes of momentum, heat, water vapor and turbulent kinetic energy at the surface and at each GCM level, as described in detail by Helfand and Labraga (1988) and Helfand and Schubert (1995). The GEOS-Terra GCM also includes the Koster-Suarez land surface model (Koster and Suarez 1992a), which is a Soil-Vegetation-Atmosphere-Transfer model based on the Simple Biosphere model of Sellers et al. (1986).

In both the standard and extended mosaic approaches, the sub-grid scale variability of the surface is modeled by viewing each GCM grid cell as a mosaic of independent vegetation stands, using linear aggregation/disaggregation formulae for links to the GCM grid. The vegetation stands, or 'tiles', interact only through the coupling to the GCM atmosphere, so there is no direct interaction between the different tiles. This modeling assumption is valid when the horizontal fluxes of heat and moisture are small compared to the vertical fluxes (Avissar and Pielke 1989; Koster and Suarez 1992a). The description of the surface in this approach is presented schematically in the lowest level of figure 1, where a hypothetical GCM grid square containing the tiles that describe the mix of surface scene types is shown. In this grid square, all of the bare soil portions of the grid box are treated as though they are juxtaposed, as are all of the deciduous trees, evergreen trees, and shrubs. Each of these types is assigned a fraction of areal coverage, and the grid box averaged quantities are computed using an area-weighted linear aggregation.

In the EM approach, the tiles are extended vertically throughout the depth of the model atmosphere. The direct influence of the surface heterogeneity is extended upwards due to the differences in the characteristics of the turbulent boundary layer above each tile. This is illustrated schematically in figure 1, where the heterogeneity at each GCM model level (LM, LM-1, etc.) is conceptualized in terms of the same tiles that characterize the surface. The air mass properties may become homogenized at any height up to or above the boundary layer height, and each individual tile retains its separate character up to that level. The underlying modeling assumption here, as an extension of the assumption neccesary at the surface layer, is that throughout the atmospheric column the tiles 'feel each other' only through the interaction with the surrounding mean flow. This assumption is valid when the horizontal turbulent fluxes throughout the depth of the boundary layer are small compared to the vertical fluxes. There is some observational justification for this assumption (Yamada 1977).

The key element to understanding the homogenization of turbulent air properties in an EM approach is the interplay between the grid-resolved processes and the tile-resolved processes. The grid-resolved processes are horizontal and vertical advection, radiative heating and cumulus convection, and the tile-resolved process is turbulent mixing. The tile space tendency due to diffusion impacts the grid space variables, and the grid scale tendencies impact the tile space variables, thus establishing the interplay.

In EM we write the total grid space tendency of an atmospheric state variable, G_α, as the sum of the tendency due to grid-space terms and the aggregated tile space terms. The terms in the equations of motion that arise from the parameterization of turbulent processes are the 'turbulent tendency' terms, and are similar for all the atmospheric state variables. In order to evaluate a turbulent tendency of an atmospheric state variable, we account for the influence of processes that occur in both grid and tile space. The grid-space tendencies are functions of grid-space variables only, while the tile-space tendencies are functions of both grid-space and tile-space variables. This can be represented by the following expression:

$$\left(\frac{\partial G_\alpha}{\partial t}\right)\bigg|_{\text{total}} = \left(\frac{\partial G_\alpha}{\partial t}\right)\bigg|_{\text{grid}} (G_{\alpha_1}, G_{\alpha_2}, ..) + \frac{1}{N}\sum_{n=1}^{N} \left(\frac{\partial G_\alpha}{\partial t}\right)\bigg|_{\text{turb}}^{n} (G_{\alpha_1}, G_{\alpha_2}, .., \mathcal{T}^n_{\beta_1}.\mathcal{T}^n_{\beta_2}, ..) * f_n,$$

where the G_α's are the grid-space state variables, the $\mathcal{T}^n_\beta$'s are the tile-space variables, and the summation is over N tiles, where 'n' is the tile index. The subscript 'grid' refers to grid-space calculations, and the subscript 'turb' refers to turbulent processes, which occur in tile space. The grid-space state variables are the horizontal components of velocity, the potential temperature, the specific humidity, the surface pressure, and any passive scalar. The tile-space variables consist of surface fields (canopy and deep soil temperatures, three levels of soil moisture, the canopy reservoir capacity, the snow depth and the canopy specific humidity) and fields defined on all GCM levels (turbulent kinetic energy and the turbulence-induced liquid water mixing ratio and cloud fraction). The second term on the right hand side of the equation contains the tile space turbulent tendency, and is proportional to the vertical divergence of the turbulent flux, namely:

$$\left(\frac{\partial G_\alpha}{\partial t}\right)\bigg|_{\text{turb}}^{n} \propto \frac{\partial}{\partial z}(\overline{w' g'_\alpha})^n,$$

where g'_α is the fluctuating component of G_α and w' is the (turbulent) vertical component of the velocity field.

In addition to the vertical extent of tile-space, there is another fundamental difference between the original mosaic approach and EM. This difference is in the handling of the tile-space surface fluxes into the bottom model layer. In EM it is the divergence of turbulent fluxes, or the turbulent tendency itself, which is computed in tile-space and aggregated for use by the GCM, whereas in mosaic the surface fluxes are aggregated, and a grid-space divergence is computed.

In a full implementation of EM the atmospheric state variables would be retained at both tile-space to compute turbulent diffusion and grid-space to compute grid-space processes. The implementation of EM described above, however, does not retain the full set of atmospheric state variables in tile space from one time step to the next, rather the tile space boundary layer structure is retained in the predicted turbulent second moments. This simplification may provide an additional homogenizing influence. To the extent that the tile space structure of the overlying boundary layer is preserved by the turbulent moments, EM as presently implemented will appropriately account for the vertical influence of surface heterogeneities.

4 The Model Blending Height

In an analogy to the blending height concept, we define here the 'model blending height' (MBH) as the model level above the heterogeneous land surface at which it is assumed that the turbulent mixing has homogenized the air mass properties. This is the level above which the flow over the different tiles begins to appear uniform. Each of the aggregation techniques described above implies a different extent of the vertical influence of surface heterogeneity in the GCM. We can view the 'composite' methodology as setting an MBH at the ground and the mosaic approach as setting an MBH at the top of the surface layer. The EM approach is the only approach that has a variable MBH.

To define a measure of the MBH we examined the results of a year-long GCM simulation using EM (see section 5 for details). Typical profiles of the turbulent fluxes of temperature, momentum and humidity over each tile in a grid box are shown in figure 2. Figure 2a shows the profiles of $\overline{w'\theta'}$ and $\overline{w'q'}$ at 3Z over a grid point located in the northern steppes (58N,75E). This particular grid box has three tiles, a broadleaf deciduous trees tile, a bare soil tile, and a needleleaf trees tile. The values of the flux emanating from the surface layer (those at the bottom $\sigma-$level) are very different from tile to tile. We also see that the differences in the turbulent fluxes between the tiles have been propagated upwards, as the fluxes are still distinct aloft. At higher levels, values of $\overline{w'\theta'}$ approach each other until approximately $\sigma = 0.975$ where the fluxes are almost indistinguishable. At this 'homogenized' level, however, the fluxes are still significant. We define the turbulent boundary layer height as the level at which the turbulent fluxes decay below 10% of their column maximum value, and this does not occur until $\sigma = 0.95$. Figure 2b shows the turbulent fluxes of momentum for the same location and time, and these are seen to exhibit the same character. This qualitative sense of the location of the MBH can be quantifed by defining a measure of the surface variability and some threshold of variability below which the fluxes over different tiles may be considered homogenized. The measure of tile-to-tile variability (V) at any level is $V = F_{\max} - F_{\min}$, where $F_{\max}$ and $F_{\min}$ are the maximum and minimum values of the turbulent flux among all the tiles, respectively. The measure of surface variability that we use is $V_s = \max(F_{\max} - F_{\min})$, where 'max' of the difference refers the the level at which the difference is maximum (usually at the surface). As we ascend in the atmospheric column, V decreases with height relative to its maximum value, V_s, and we define the MBH as the level at which it descends below the threshold.

To determine the proper threshold, profiles of turbulent fluxes and the resulting MBH were examined under many atmospheric and geographic conditions. The threshold varies with the magnitude of our measure of the surface variability, V_s. The thresholds are listed in table 1. For the vast majority of profiles and conditions (88 % of the total points), the threshold value for V is 20% of V_s. For the profiles in figures 2a and b, the 20% threshold resulted in an MBH at $\sigma = 0.975$, which is indeed where the fluxes begin to appear uniform. For conditions under which the fluxes and the surface variability were large (> 0.2 kg m^{-2} s^{-1} $^\circ K$ for heat fluxes), such as seen in figure 2c, a threshold of 20% would place the MBH at $\sigma = 0.955$, which is clearly too low. For these profiles, (roughly 7% of the total points), the threshold used is 5% of V_s. In contrast, when the fluxes and the surface variability were small (< 0.006 kg m^{-2} s^{-1} $^\circ K$), such as seen in figure 2d, the 20% threshold would set the MBH at $\sigma = 0.935$ which is clearly too far above the level at which the fluxes merge. For these profiles, (roughly 4% of the total points), the threshold used is 65% of V_s, and the MBH is at $\sigma = 0.985$. Another threshold of 80% of V_s was needed for the roughly 1% of the cases in which V_s is very small (< 0.001 kg m^{-2} s^{-1} $^\circ$ K). With this choice of threshold, along with our choice of V_s as the measure of surface variability, we chose to define the MBH based on heat fluxes alone. Calculations of the MBH were also performed based on the moisture and momentum fluxes, and the resulting values were almost indistinguishable from those based on the heat fluxes.

Our algorithm to estimate the MBH is consistent with the ideas used to estimate the blending height (Mahrt 2000). These different approaches to assessing a measure of the level of the blending height all involve some measure of the surface variability and the level at which it decays below some threshold. One such measure involves a threshold value for the variance of the skin temperature normalized by some reference potential temperature, σ_{T_s}/Θ_0. Another measure involves the variance of *some* turbulent flux divided by the flux, σ_F/F. In the context of our GCM study using the variance as the measure of surface variability is not suitable for a mosaic scheme involving 3-4 tiles in a grid box. Just like our measure of the surface variability, these measures of surface variability do not dependant exclusively on the vegetation characteristics themselves. The physical characteristics of the land surface, such as the surface roughness and the soil hydraulic conductivity, are constant in time or vary on monthly time scales. The measures defined above depend on the local conditions as well, which may vary on many shorter and longer time scales. For example, under extreme cold atmospheric conditions the surface fluxes are minimal, and under wet conditions the evaporation proceeds at its potential rate. Either of these conditions will result in the suppression of any differences in physical characteristics and a reduced surface variability.

5 Characterization of the MBH

We now examine the spatial and temporal variability of the MBH and the relationship with other quantities using a year-long segment of a 27 month simulation performed with the EM technique as implemented in the GEOS-Terra GCM. The simulation is from December, 1997 to March, 2000, and is forced with observed weekly varying sea surface temperatures. The surface types used in this experiment are listed in table 2, and the data for percent of the grid cell occupied by any surface type were derived from the surface classification of Defries and Townshend (1994), and information about the location of permanent ice was obtained from the classifications of Dorman and Sellers (1989). The resulting vegetation map can be found in figure 2 of Molod and Salmun (2002). In general, most grid boxes are characterized by approximately four different scene types (tiles). Several of the vegetation characteristics, namely the leaf area index, greenness fraction and surface roughness length, vary from month to month, while the others are constant throughout the year. The simulation results of 1998, for which an extensive diagnostic output in tile space was generated, were used to examine the EM technique by analyzing the behavior of the MBH. We focus on the relationships between the MBH and other relevant physical parameters, such as the planetary boundary layer (PBL) height, the surface temperature and fluxes, and the type and distribution of underlying vegetation. To illustrate these relationships, we will present monthly averages of global fields and annual time series for representative points around the globe.

DJF seasonal mean values of MBH, PBL, and the ratio MBH/PBL, given in pressure thickness above the surface, are shown in figure 3. These plots show that the MBH is variable, is above the surface layer, and is related to the PBL height but does not follow it exactly. The values of MBH range from 10 mb to near 40 mb (100m to 400m, approximately). The geographic locations where the MBH is low, which are indicated by the blue areas of figure 3a, are the Tibetan plateau, the Rocky Mountains, the Amazon basin, Central Africa and Siberia. The low MBH corresponds to low PBL values (the light blue regions in figure 3b) in all of these regions except for the Amazon, where the low MBH is associated with a relatively homogeneous terrain. Regions where the MBH is high during DJF are the southern hemisphere mid-latitude areas, where it is summertime, and where the PBL values are also high. There is another band of high MBH values at approximately 45^oN latitude across the North American, European and Asian continents. There is some indication of a local maximum in PBL height at these locations, as well as a transition of vegetation types at that latitude. There is also a local maximum in MBH in the Sahel region of Africa, related to the behavior of the PBL.

The ratio of MBH to PBL is always less than 1 (figure 3c), ranging from 0.05 to greater than 0.9, indicating that the MBH is always below the PBL. The global mean ratio is approximately $0.2 - 0.3$. There is a monotonic decrease in the ratio of MBH to PBL in the Northern Hemisphere from high latitudes (ratio near 0.9) to low latitudes (ratio near 0.15), except in the eastern United States. The large change in ratio is the result of a PBL thickness which increases more rapidly than the MBH from north to south across these regions. In general, the ratio is low in the Southern Hemisphere, due to the high summertime PBL values. There is a local minimun in the ratio over eastern US, which corresponds to the local maximum in the PBL height (with a similar contour shape). In addition, there is a local minimum in the ratio over Sahel, where the PBL height is very high (greater than 300 mb). The ratio increases north of Sahel, due to the more rapid dropoff of the PBL height than the MBH.

The corresponding plots for June-July-August (JJA) are shown in figure 4. These plots also show that the MBH is variable, and lies above the surface layer and inside the PBL. Some of the areas where the MBH is high correspond to high PBL values, such as the deserts of Sahara, Gobi, Saudi Arabia and southwestern United States, and regions in southern Africa and just south of the Amazon. An additional band of high MBH values exists at approximately $35^o - 40^o$N latitude, stretching across Canada, Europe and Asia. These high MBH values do not correspond to local maxima in the PBL height, rather they correspond in the shape of the contour to areas where there is a change in the nature of the vegetation (see figure 2 of Molod and Salmun 2002). In these regions the vegetation changes from a combination of bare soil and dwarf trees to predominantly needleleaf trees. The geographical locations where the MBH is low are the Amazon, where the variability of the vegetation is small, and the Andes and the Tibetan Plateau, where the altitude and the cold temperatures limit the height of the PBL. There is also a local minimum in MBH in the southern tip of Africa, and another in central South America, just south of the local maximum. The ratio of MBH to PBL values is generally lower than in the northern hemisphere wintertime, with the lowest values (less than 20%) corresponding to the highest values of PBL height. Except for Southern Africa, the ratios are higher in the southern hemisphere (winter hemisphere) than in the summer hemisphere.

In general the MBH values differ more from the PBL height values in JJA than in DJF. The evolution of these fields throughout the year (not shown) indicates that the latitude of maximum MBH in the northern hemisphere traverses poleward in the wintertime and equatorward in summertime. This can be seen in the DJF and JJA MBH fields, where, for example over Asia, the location of high MBH values (shaded orange in the figure, 30-35 mb) is near 60N latitude in DJF, and moves south to near 40N in JJA. The same summer-winter traverse can be seen in Africa and South America from DJF to JJA, but in the southern hemisphere the poleward shift occurs in the summertime (December).

To gain some further insight into the relationship between the MBH and the PBL, we examine scatter plots of seasonal mean MBH versus PBL for all land points. Figure 5 shows this plot for JJA. In general, the MBH increases with PBL height, except for high (greater than 200 mb) PBL values, where there is a leveling off of the MBH. These high PBL values occur over desert areas, where the variability of the surface vegetation is small (90% desert and 10% broadleaf shrubs), and in a small area in the Amazon, the behavior of which is examined below. Although there is a linear trend between MBH and PBL for the lower PBL values, the spread about the representative line is greater than 2 standard deviations. This spread indicates that the MBH does not depend simply on PBL height, but is the result of a more complex interplay among different physical processes. Similar behavior was observed in DJF (not shown).

We examined the involvement of the other physical processes in determining the MBH by examining similar scatter plots for other variables. Figure 6 shows the scatter plot of JJA MBH against T_c. It shows that the MBH increases with T_c, with MBH values ranging from near 10 mb to near 45 mb over a temperature range of 260^oK to 310^oK. The exception to this behavior is a small group of points, colored in red, at relatively warm canopy temperatures (just below 300^oK), for which the MBH values are near 10-15 mb, rather than closer to 30 mb, as the global trend would have dictated. These points are all characterized as tropical rain forest, and the relationship between MBH and T_c over this type of densely forested terrain is markedly different from the relationship over other types of soil and vegetation. For these points, the MBH varies much more rapidly with temperature and ranges from 13 mb to 42 mb over a T_c range of 295^oK to 300^oK. In the tropical rain forests, the low MBH (and lower T_c) points are characterized by very high levels of evaporation, and the high MBH (and higher T_c) points have almost no evaporation. We illustrate this behavior with contour plots of MBH, T_c and turbulent surface fluxes over the Amazon region, figures 7a-d, where we see that the areas of high MBH (figure 7a) correspond to the areas of low evaporation (figure 7c). At the lower temperatures, the evaporation levels suppress the sensible heat flux (available energy at the surface is released through evaporation, primarily through evapotranspiration) and the MBH is lower. In contrast, at the higher temperatures (beyond the model-specified threshold), the evaporation is suppressed to conserve leaf and plant moisture, the sensible heat flux is increased, and the MBH is higher. This correspondence to the sensible heat flux is seen in figure 7d.

Similar scatter plots of MBH versus sensible heat flux (not shown) show that the global relationship between the MBH and the sensible heat flux is linear in character, with MBH increasing with sensible heat. This is as expected, given that the sensible heat flux is the major contributor to the boundary layer bouyancy and turbulence which determines the PBL height. This relationship between MBH and sensible heat flux is independent of the choice of surface variability used to define the MBH. The linear relationship holds even when the MBH is defined based on the variability of surface latent heat flux or momentum flux.

In addition to a relationship between the MBH and the local characteristics of the turbulence, the behavior of the MBH also depends on the type and variability of surface vegetation. We demonstrate this relationship with a year-long time series of the MBH and PBL at two characteristic points in the region of the Indian/Asian monsoon. These points and their vegetation characteristics are indicated in figure 8, which shows a shaded map of the fractional area covered by vegetation types *other* than the dominant type. This is a measure of the variability of vegetation in the grid box. The first point is in southern Asia (100E, 16N) and is characterized by 60.0% groundcover, 14.8% broadleaf evergreen trees, 14.3% broadleaf deciduous trees, 8.9% bare soil and 2.0 % dwarf trees. This point has the higher off-dominant percent of coverage of the two points, and is also differentiated from the other point by the presence of the deciduous trees. The second point is on the Indian subcontinent (77.5E, 12N) and is characterized by 80.5% groundcover, 9.8% bare soil, 4.7% dwarf trees, 3.1% broadleaf deciduous trees, and 1.9% broadleaf evergreen trees. This point has the lower off-dominant fraction and almost no deciduous trees. Both of these points are in climatologically similar regimes, governed by a monsoonal flow and relatively dry in the wintertime. Figure 9 shows a 1-day and 30-day running mean of the PBL (9a and 9c) and MBH (9b and 9d) for the two points. The PBL at both points shows a robust seasonal cycle, high (near 140 mb) in the springtime and low (near 40 mb) in the winter. The MBH, however, exhibits distinctly different behavior between the two points. Figure 9b shows that the point with higher vegetation variability and the higher amount of deciduous trees (100E,16N) has a marked seasonality in the MBH, ranging from near 40 mb in the late spring (lagging behind the PBL by a month) to approximately 20 mb in the fall. In contrast, the other point (77.5E,12N) shows no such seasonality in the MBH, as seen in figure 9d. The value of the MBH is nearly constant at 25 mb throughout the year.

Examination of time series of some other relevant meteorological fields aids in understanding the connection between the presence of deciduous trees and the MBH seasonality. Figure 10 shows the 1-day and 30-day running means of the latent heat flux (10a,b), canopy temperature (10c,d), precipitation (10e,f) and sensible heat flux (10g,h) for both points. The similarity of the precipitation patterns (figures 10e and 10f) and canopy temperature patterns (10c and 10d) at both points demonstrates that they are in the same climate regime. Figures 10a and 10b show that the latent heat flux over the point with deciduous trees is almost completely suppressed during the months when the trees have no leaves. This results in a sharper increase in latent flux during the springtime. In contrast, at 77.5E,12N (the point with no deciduous trees and low surface variability) the latent flux is small in wintertime but is not completely suppressed, and the contrast between winter and springtime levels is not as marked. Consistent with the behavior of the latent heat flux, figures 10g and 10h show that the sensible heat flux at 100E,16N is higher in wintertime than the sensible heat at 77.5E,12N.

Examination of other points in this climatological regime revealed that the presence of deciduous trees alone is insufficient to generate a high seasonality in the MBH. High surface variability is necessary as well. For example, the grid box at 77.5E, 10N has deciduous trees but low surface variability, is characterized by 80.0% groundcover, 9.0% broadleaf deciduous trees, 10.0% bare soil, and 1.0 % dwarf trees, and shows no seasonality in the MBH, despite a marked seasonality in the PBL. In other words, the variability and the presence of deciduous trees is needed for the MBH to exhibit a strong seasonal cycle.

6 Summary and Conclusions

The study of the extended mosaic technique presented here is aimed at developing a better tool to simulate and understand the interactions between a heterogeneous land surface and the climate. This technique allows the influence of the surface heterogeneities to extend upwards into the turbulent boundary layer by assuming that the conceptualization of surface heterogeneity as a mosaic of independent vegetation stands is applicable throughout the atmospheric column. The additional degree of freedom of the system, that of allowing the vertical extent of the influence of surface heterogeneities to be determined internally, has the potential to afford a better characterization of the land-atmosphere interactions.

Simulations with this technique revealed that the profiles of turbulent fluxes over each tile in a grid box differ near the ground and become homogenized at some level aloft. This behavior allows the definition of a 'model blending height' (MBH) as the level where the homogenization takes place. We emphasize that the EM algorithm does not require that the turbulent fluxes become homogenized, hence the blending is a *result* of the simulations with EM. The MBH varies was between 50 and 500 meters, and is generally about one third of the PBL height. The exact ratio depends on climatological and meteorological conditions, location and the amount of variability in the land scene type.

Examination of the relationship among the MBH and other meteorological variables shows that seasonal mean values of the MBH and PBL height exhibit similiar spatial patterns in warm and dry regions, and differ more in the northern hemisphere wintertime and over relatively homogeneous terrain. The MBH increases gradually with PBL height, sensible heat flux, and canopy temperature through moderate to warm values, although the spread of values about these trends is substantial. This spread is indicative of the complexity of the dependence of the MBH on local and climatological conditions, and several examples of this complexity were presented.

The dependance of the MBH on the canopy temperature increases dramatically for temperatures near 300 ^{o}K. This is related to the behavior of the latent heat flux, which is high for temperatures just below 300 ^{o}K, and is suppressed (infinite stomatal resistance) when the canopy temperature exceeds a vegetation-dependent threshold (usually near 300 ^{o}K). When the evaporation is high, the MBH is low, and when the available surface energy is released as sensible rather than latent heat flux, the MBH is elevated. This results in the sharp increase of MBH with canopy temperature in regions where evaporation dominates the surface energy balance.

The MBH was also found to depend on the variability and types of underlying vegetation. The presence of deciduous trees in the mix of tiles, in addition to high levels of variability in scene type, was shown to be associated with in an increased seasonality of the MBH. An example of this behavior was presented by examining two grid boxes in similar climate regimes (monsoonal circulation), where the annual cycle of evaporation (and sensible heat flux) is significantly enhanced at the grid box which contains deciduous trees.

In this study we have presented a physically consistent depiction of the relationship between the MBH and the turbulent boundary layer overlying a heterogeneous surface. However, the robustness of the model results must still be determined by comparisons against observational and high resolution model estimates of the blending height. To facilitate the comparison against this type of verification data, and to better understand the mechanisms at work, we will further examine the details of the behavior of the MBH and attempt to develop a scaling relationship for the dependance on local and climate variables. We are currently investigating the impact of the EM technique on simulated land-atmosphere feedbacks by comparing parallel simulations with EM and a more standard mosaic approach, and evaluating any differences in the context of available climatological observations.

Acknowledgements. AM gratefully acknowledges discussions with Max Suarez, Mark Helfand and Randal Koster which were helpful in the development of the extended mosaic technique. Sharon Nebuda also provided invaluable day to day support during the development stages of the technique. The authors are grateful for the general support and encouragement given to us by Paul Houser and Randal Koster for the ideas presented in this paper. The computing resources for these experiments were provided by the NASA Data Assimilation Office. AM is supported by NASA Earth System Science Graduate Fellowship ESS/00-0000-0016

References

Arola, A. and D. P. Lettenmaier, 1996: Effects of Subgrid Spatial Heterogeneity on GCM-Scale Land Surface Energy and Moisture Fluxes. *J. Climate*, **9**, 1339-1349.

Avissar, R., and R. Pielke, 1989: A parameterization of heterogeneous land surfaces for atmospheric numerical models and its impact on regional meteorology. *Mon. Wea. Rev.*, **117**, 2113-2136.

Avissar, R., 1991: A statistical-dynamical approach to parameterize subgrid-scale land-surface heterogeneity in climate models. In Wood, E.F. (ed.), *Land Surface-Atmosphere Interactions for Climate Modelling*, Kluwer Academic Publishers, Dordrecht, pp. 155-178.

Betts, A. K. and M. Miller, 1986: A New Convective Adjustment Scheme. 2. Single Column Tests using GATE WAVE, BOMEX, ATEX and Arctic Air Mass Data Sets. *Quart. J. Royal Met. Soc.* **112**, 693-709.

Bringfelt, B., 1999: A New Land-Surface Treatment for HIRLAM - Comparisons with NOPEX Measurements. *Agr. Forest Meteorol.*, **98-9**, 239-256.

Brutsaert, W., 1998: Land-surface water vapor and sensible heat flux: spatial variability, homogeneity, and measurement scales. *Water Res. Res.*, **34**, 2233-2442.

Claussen, M., 1995: Flux Aggregation at Large Scales: On the Limits of Validity of the Concept of Blending Height. *J. Hydrol.* **166**, 371-382.

DeFries, R., M. Hansen, J. R. G. Townshend, A. C. Janetos and T. R. Loveland, 2000: A New Global 1 km dataset of Percent Tree Cover Derived from Remote Sensing. *Global Change Biology*, **6**, 247-254.

DeFries, R. S. and J. R. G. Townshend, 1994: NDVI-derived land cover classification at global scales. *Intl J. of Remote Sensing*, **15**, 3567-3586, Special Issue on Global Data Sets.

Dickinson, R. and P. Kennedy, 1992: Impacts on regional climate of Amazon deforestation. *Geophys. Res. Letters.*, **19**, 1947-1950.

Dickinson, R., A. Henderson-Sellers, P. Kennedy and M. Wilson, 1986: Biosphere-Atmosphere Transfer Scheme (BATS) for NCAR Community Climate Model. *Tech. Note TN 275+STR*, 69pp., Nat.Cent. for Atmos. Res., Boulder, Colo.

Dorman, J. L., and P. J. Sellers, 1989: A global climatology of albedo, roughness length and stomatal resistance for atmospheric general circulation models as represented by the Simple Biosphere model (SiB). *J. Appl. Meteor.*, **28**, 833-855.

Entekhabi, D. and P. S. Eagleson, 1989: Land surface hydrology parameterization for atmospheric general circulation models including subgird scale spatial variability. *J. Climate* **2**, 816-831.

Garrat, J. R., 1980: Surface influence upon vertical profiles in the atmospheric near surface layer. *Quart. J. Royal Met. Soc.* **106**, 803-819.

Gates, W. L. (ed.), 1995: The Proceedings of the First International AMIP Scientific Conference. *WCRP-92, WMO/TD-No. 732*, World Climate Research Programme, World Meteorological Organization, Geneva, 532pp.

Giorgi, F. and R. Avissar, 1997: Representation of Heterogeneity Effects in Earth System Modeling: Experience from Land Surface Modeling. *Rev. Geophys.*, **35**, No 4, 413-438.

Helfand, H. M., M. and S. D. Schubert, 1995: Climatology of the Simulated Great Plains Low-Level Jet and Its contribution to the Continental Moisture Budget of the United States. *J. Climate*, **8**, 784-806.

Helfand, H. M., and J. C. Labraga, 1988: Design of a non-singular level 2.5 second-order closure model for the prediction of atmospheric turbulence. *J. Atmos. Sci.*, **45**, 113-132.

Henderson-Sellers, A., R. Dickinson, T. Durbidge, P. Kennedy, K. McGuffie and A. Pitman, 1993: Tropical deforestation: modeling local to regional scale climate change. *J. Geophys. Res.,*, **98**, 7289-7315.

Henderson-Sellers, A. and A. J. Pitman, 1992: Land-Surface Schemes for Future Climate Models: Specification, Aggregation, and Heterogeneity. *J. Geophys. Res.*, **97**, 2687-2696.

Himaya, T., M. Sugita and K. Kotoda, 1996: Regional roughness parameters and momentum fluxes over a complex area. *J. Appl. Meteor.* **35**, 2179-2190.

Houser, P. R., R. Yang, J. Joiner, A. DaSilva and S. Cohn, 1997: Land Surface GEOS Modeling and Data Assimilation Strategy, DAO Office Note 1997-??, Office Note Series on Global Modeling and Data Assimilation, Goddard Space Flight Center, Greenbelt, MD 20771, 21pp.

Klink, K., 1995: Surface Aggregation and Subgrid-Scale Climate. *Int. J. Climatol.*, **15**, 1219-1240.

Koster, R. D., and M. J. Suarez, 1992a: Modeling the Land Surface Boundary in Climate Models as a Composite of Independant Vegetation Stands. *J. Geophys. Res.*, **97**, 2697-2715.

Koster, R. D., and M. J. Suarez, 1992b: A Comparitive Analysis of Two Land Surface Heterogeneity Representations. *J. Climate*, **5**, 1379-1390.

Koster, R. D., and M. J. Suarez, 1992c: Energy and Water Balance Calculations in the MOSAIC LSM. NASA Technical Memorandum 104606 Volume 9, Technical Report Series on modeling and Data Assimilation, Max J. Suarez, ed., Goddard Space Flight Center, Greenbelt, MD 20771, 76 pp.

Lord, S. J., 1982: The Interaction of a Cumulus Cloud Ensemble with the Large Scale Environment. 3. Semi-prognostic tests of the Arakawa-Schubert Cumulus Parameterization. *J. Atmos. Sci.*, **39** , 88-103.

Mahrt, L., 2000: Surface Heterogeneity and Vertical Structure of the Boundary Layer. *Boundary-Layer Meteorol.* **96**, No. 1-2, 33-62.

Mahrt, L., 1996: The Bulk Aerodynamic Formulation Over Heterogeneous Surfaces. *Boundary-Layer Meteorol.* **78**, 87-119.

Mason, P. J., 1988: The formation of areally-averaged roughness length. *Q. J. R. Meteorol. Soc.*, **114**, 399-420.

Mölders, N, A. Raabe and G. Tetzlaff, 1996: A Comparison of Two Strategies on Land Surface Heterogeneity Used in a Mesoscale β Meteorological Model. *Tellus*, **48A**, 733-749.

Molod, A., and H. Salmun, 2002: A Global Assessment of the Mosaic Approach to Modeling Land Surface Heterogeneity. *J. Geophys. Res.*, *In Press.*

Molod, A., 1999: The Land Surface Component in GEOS: Model Formulation. DAO Office Note 1999-03, Office Note Series on Global Modeling and Data Assimilation, Goddard Space Flight Center, Greenbelt, MD 20771, 21pp.

Molod, A., Helfand, H. M., and L. L. Takacs, 1996: The Climatology of Parameterized Physical Processes in the GEOS-1 GCM and their Impact on the GEOS-1 Data Assimilation System. *J. Climate*, **9** , 764-785.

Parlange, M. B. and G. Katul, 1995: Watershed scale shear stress from tethersonde wind profile measurements under near neutral and unstable atmospheric stability. *Water Resour. Res.* **31**, 961-968.

Polcher, J. and K. Laval, 1994: The impact of African and Amazonian deforestation on tropical climate. *J. Hydrol.*, **155**, 389-405.

Randall, D. A., K. M. Xu, R.J.C. Somerville and S. Iacobellis, 1996: Single Column models and Cloud Ensemble models as links between obdservations and climate models. *J. Clim.*, **9**, 1683-1697.

Raupach, R. R. and J. J. Finnegan, 1995: Scale Issues in Boundary-Layer Meteorology: Surface Energy Balances in Heterogeneous Terrain. *Hydro. Proc.*, **9**, 589-612.

Schubert, S. D., C.-K. Park, C.-Y. Wu, R. W. Higgins, Y. Kondratyeva, A. Molod, L. L. Takacs, M. Seablom and R. Rood, 1995: A Multi-Year Simulation with the GEOS-1 System: Overview and Results. NASA Tech. Memo 104606 Volume 6, NASA/Goddard Space Flight Center, Greenbelt, MD, 183 pp.

Schubert, S. D., J. Pfaendtner and R. Rood, 1993: An assimilated data set for Earth Science applications. *Bull. Amer. Meteor. Soc.*, **74**, 2331-2342.

Sellers, P. J., Y. Mintz, Y. C. Sud and A. Dalcher, 1986: A Simple Biosphere Model (SiB) for Use within General Circulation Models. *J. Atmos. Sci.*, **43**, 505-531.

Wieringa, J., 1986: Roughness-dependent geographical interpolation of surface wind speed averages. *Q. J. R. Meteorol. Soc.*, **112**, 867-889, 1986.

Yamada, T., 1977: A Numerical Simulation of Pollutant Dispersion in a Horizontally-Homogeneous Atmospheric Boundary Layer. *Atmos. Environ.*, **11**, 1015-1024.

List of Captions

Threshold Values used to determine the MBH

V_s	Threshold %
$V_s < 0.001$	80
$0.001 < V_s < 0.006$	65
$0.006 < V_s < 0.2$	20
$0.2 < V_s$	5

Table 1

GEOS-Terra GCM Surface Type Designation

Type	Vegetation Designation
1	Broadleaf Evergreen Trees
2	Broadleaf Deciduous Trees
3	Needleleaf Trees
4	Ground Cover
5	Broadleaf Shrubs
6	Dwarf Trees (Tundra)
7	Bare Soil
8	Desert (Bright)
9	Glacier
10	Desert (Dark)
100	Ocean

Table 2

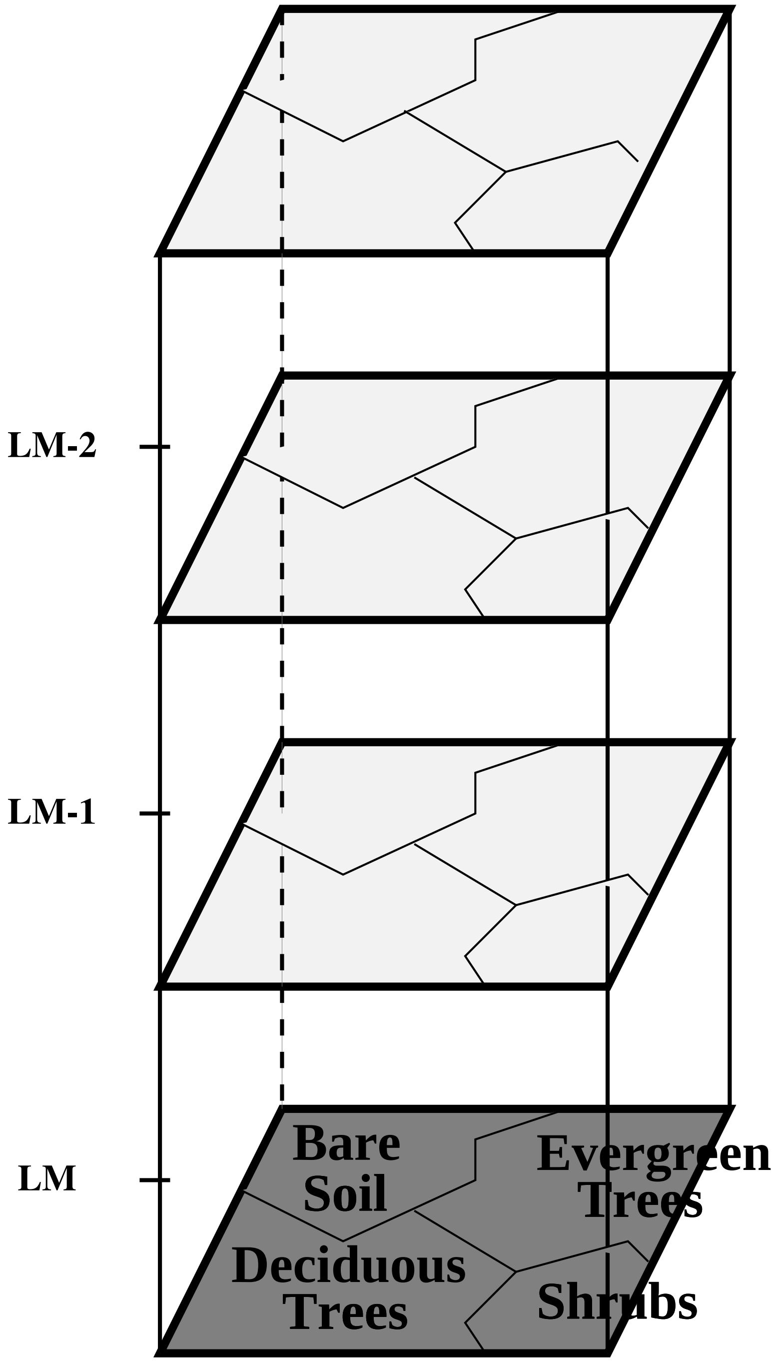

Figure 1: Schematic of the Extended Mosaic technique. The vertical axis indicates the GCM model levels, where LM is the lowest level and the level number decreases as we ascend in the column.

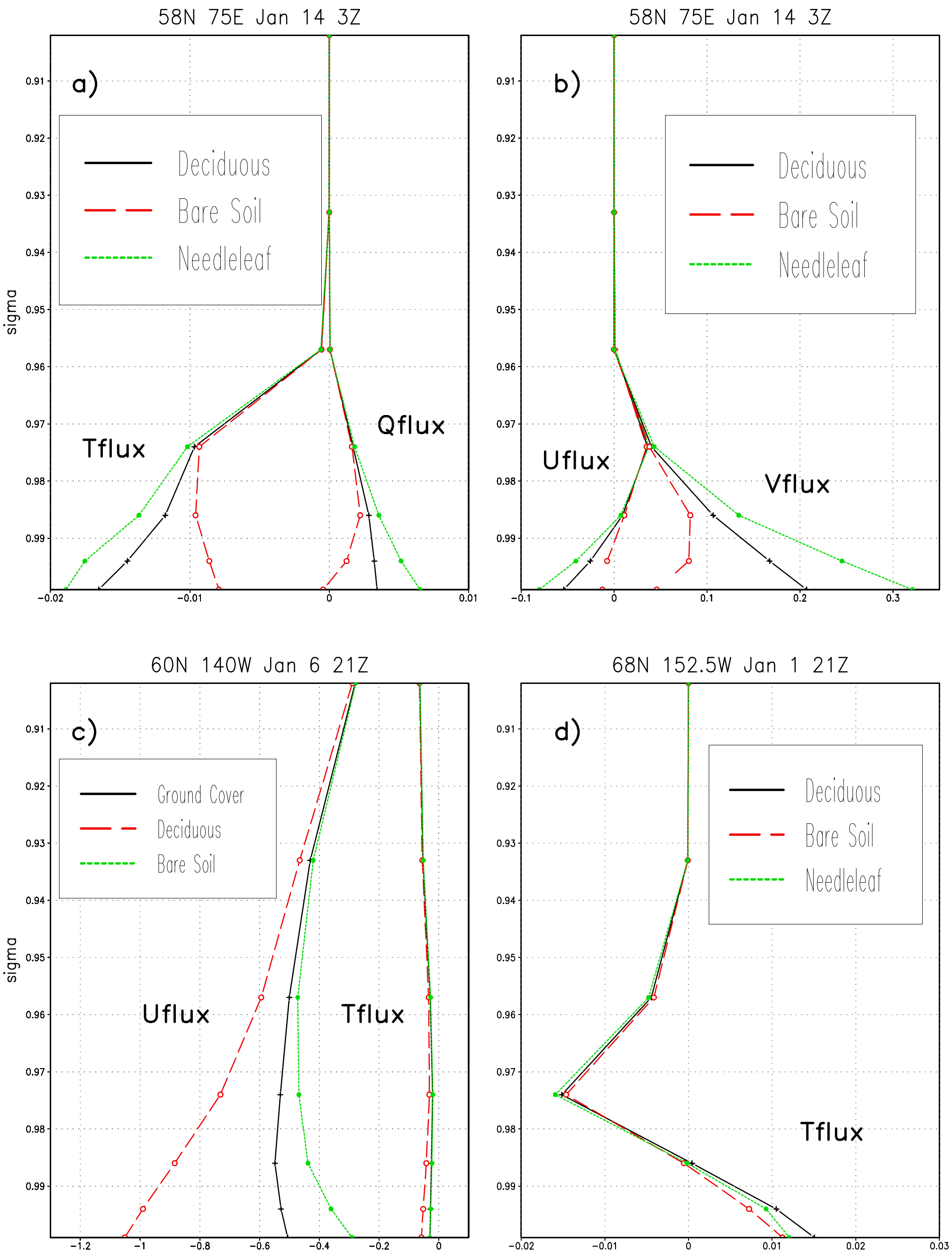

Figure 2: Typical turbulent flux profiles for the tiles in a grid box. a) Heat and moisture flux, and b) u-momentum and v-momentum flux for typical values of V_s, c) heat and momentum flux for a case in which V_s is large, and d) heat flux for a case in which V_s is small. The units of the horizontal axis indicate the value of the appropriate turbulent flux, where heat flux is in kg m^{-2} s^{-1} °K, moisture flux is in kg m^{-2} s^{-1} dg kg^{-1}, and momentum flux is in kg m^{-1} s^{-2}. The vertical axis is model σ level, which can be multiplied by 1000 to approximate pressure in mb.

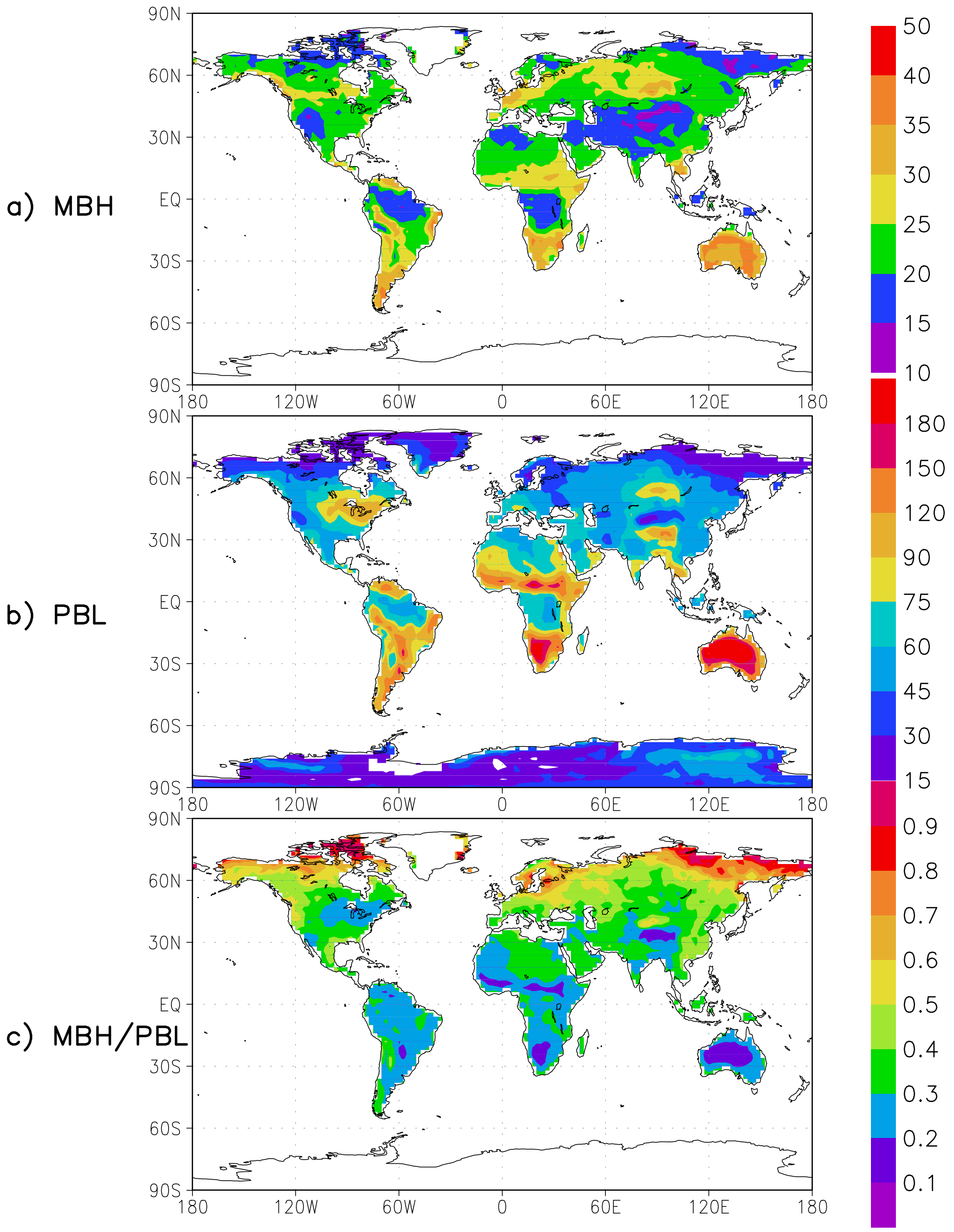

Figure 3: December-January-February averaged Model Blending Height and Planetary Boundary Layer depth. a) Model Blending Height in mb, b) Planetary Boundary Layer depth, also in mb, and c) ratio of MBH to PBL (dimensionless). The contour levels are indicated in the color bar to the right of each panel.

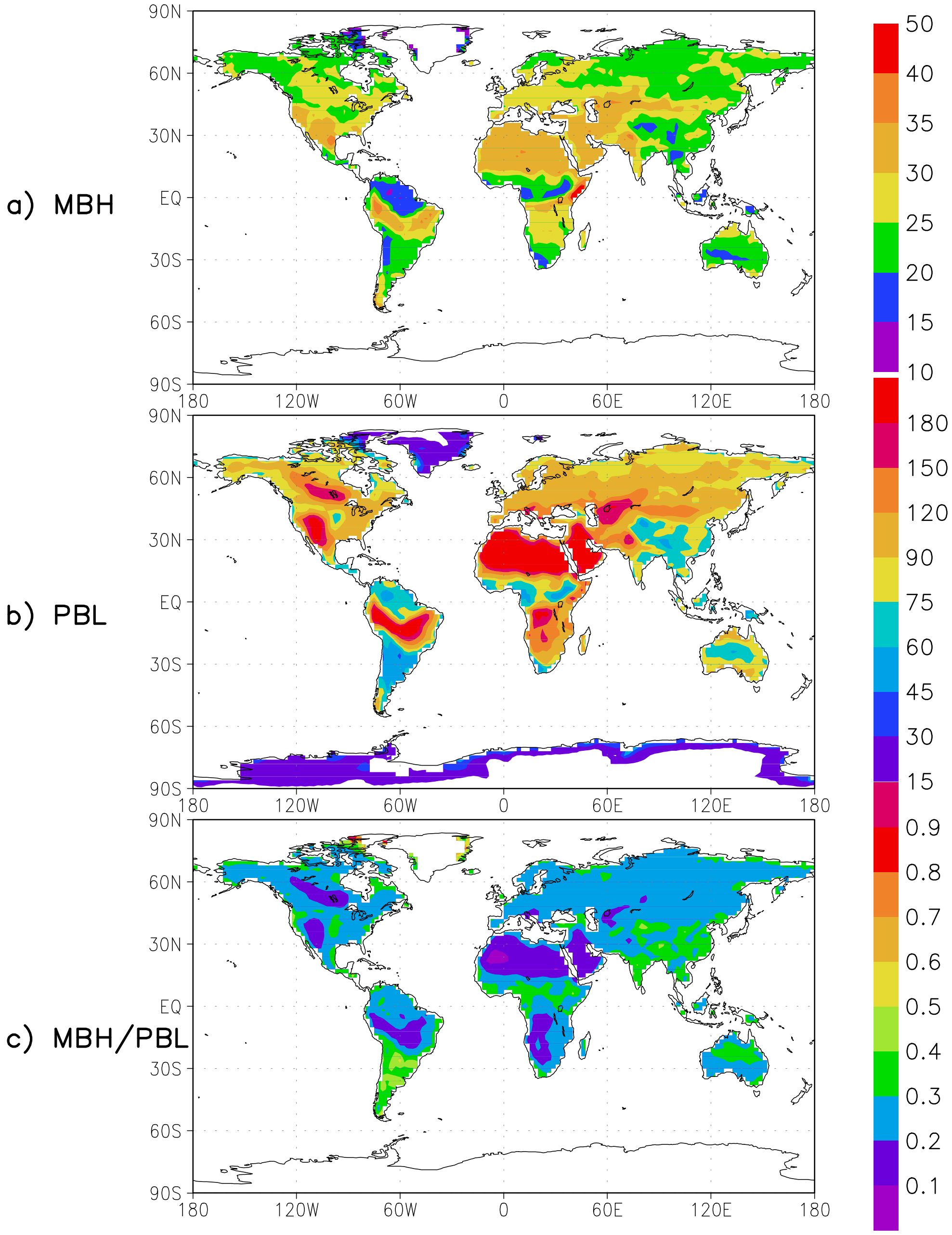

Figure 4: June-July-August averaged Model Blending Height and Planetary Boundary Layer depth. a) Model Blending Height in mb, b) Planetary Boundary Layer depth, also in mb, and c) ratio of MBH to PBL (dimensionless). The contour levels are indicated in the color bar to the right of each panel.

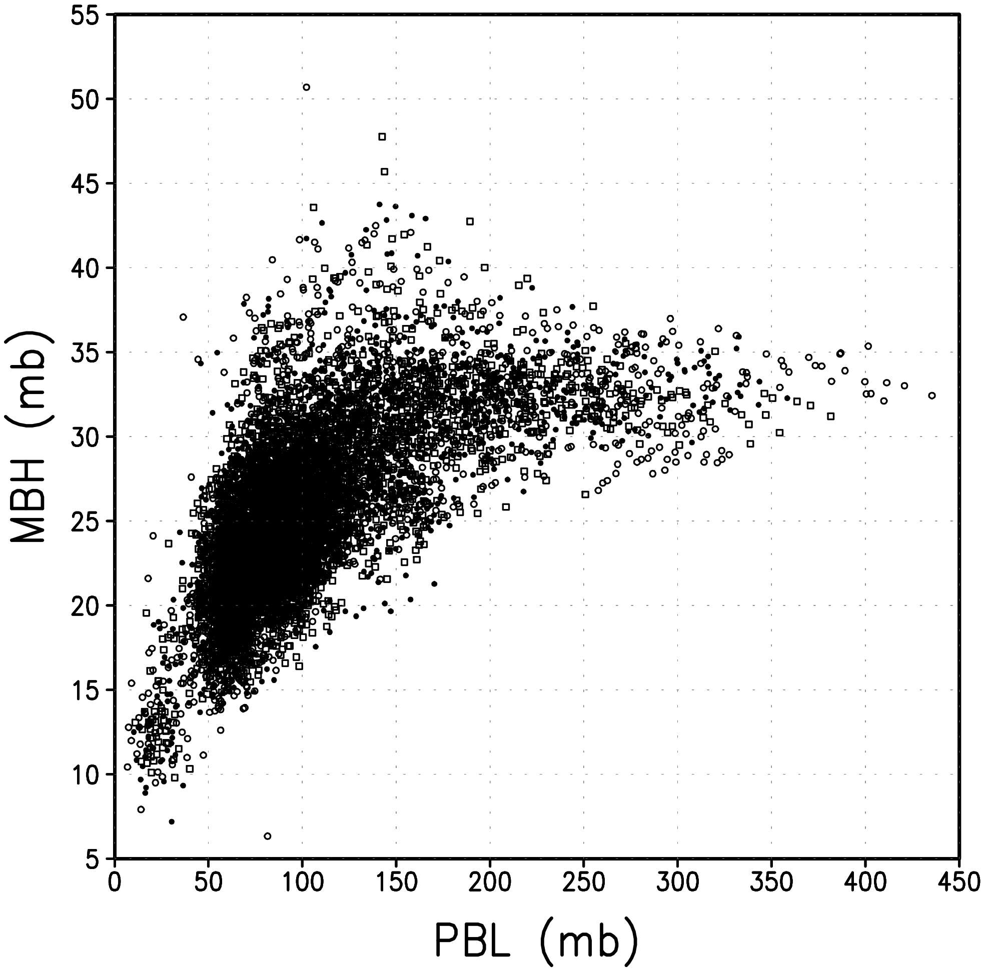

Figure 5: MBH versus PBL scatter plot (in mb) for June, July and August monthly mean values over all land points.

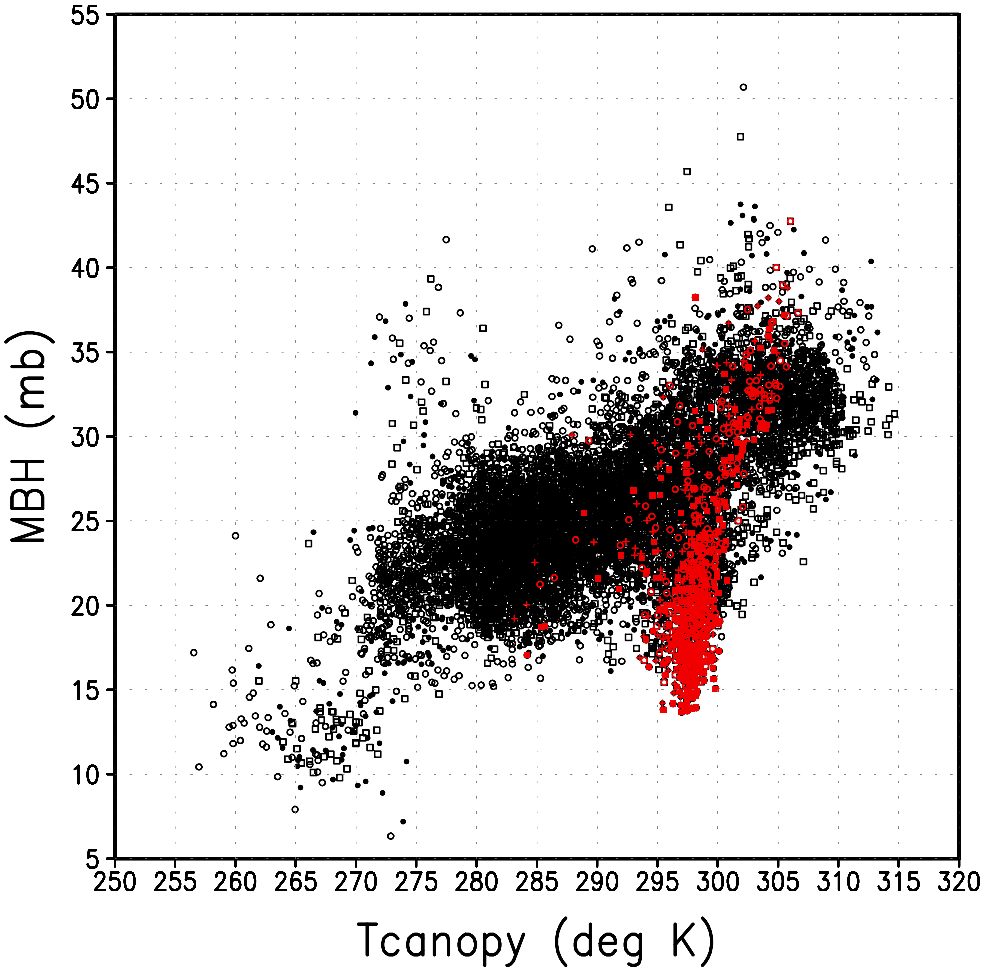

Figure 6: MBH (mb) versus canopy temperature ($^{\circ}K$) scatter plot for June, July and August monthly mean values over all land points. Points over tropical rain forests are colored red.

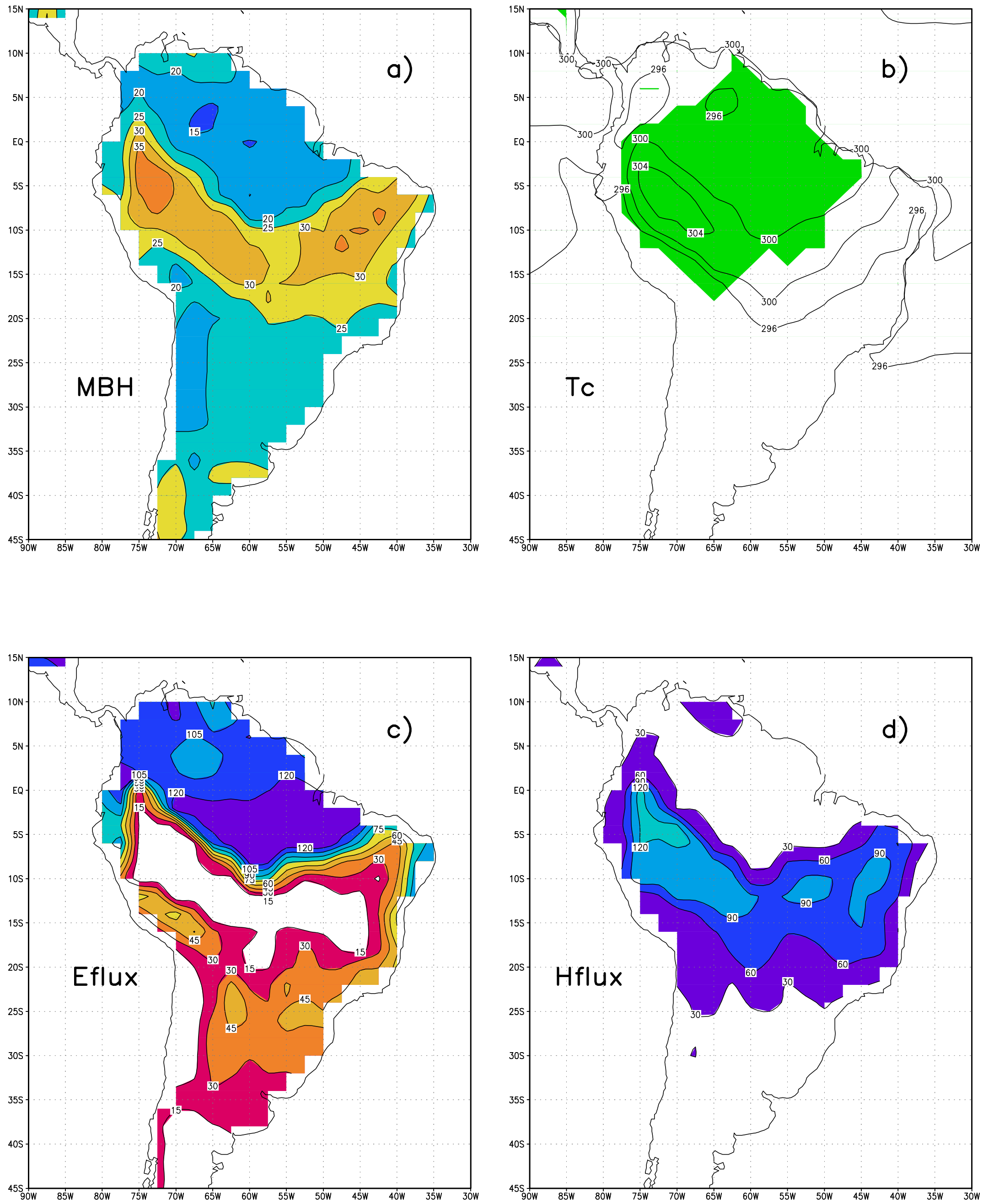

Figure 7: June, July, August seasonal mean contour plots for South America. a) MBH in mb, contour interval is 5 mb, b) canopy temperature in $^\circ K$, contour interval is 4 $^\circ K$, c) latent heat flux in W m^{-2}, contour interval is 15 W m^{-2}, and d) sensible heat flux in W m^{-2}, contour interval is 30 W m^{-2}. The area shaded green in panel b) corresponds to the area covered by tropical rain forest.

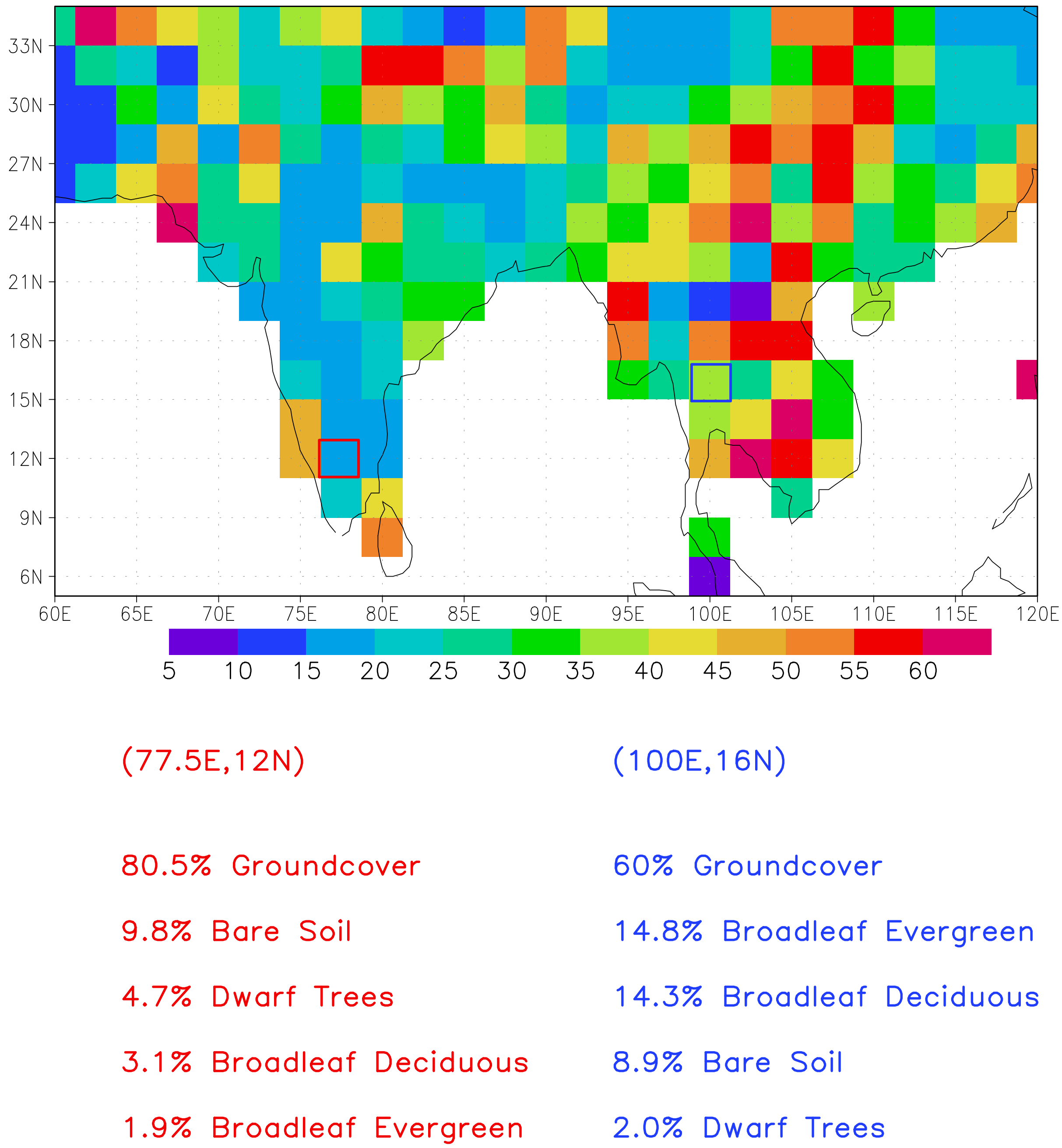

Figure 8: Percent of grid box covered by non-dominant vegetation for southern Asia. The two grid points chosen for illustration are indicated by the blue and red boxes in the figure, and by the description of vegetation characteristics below the map.

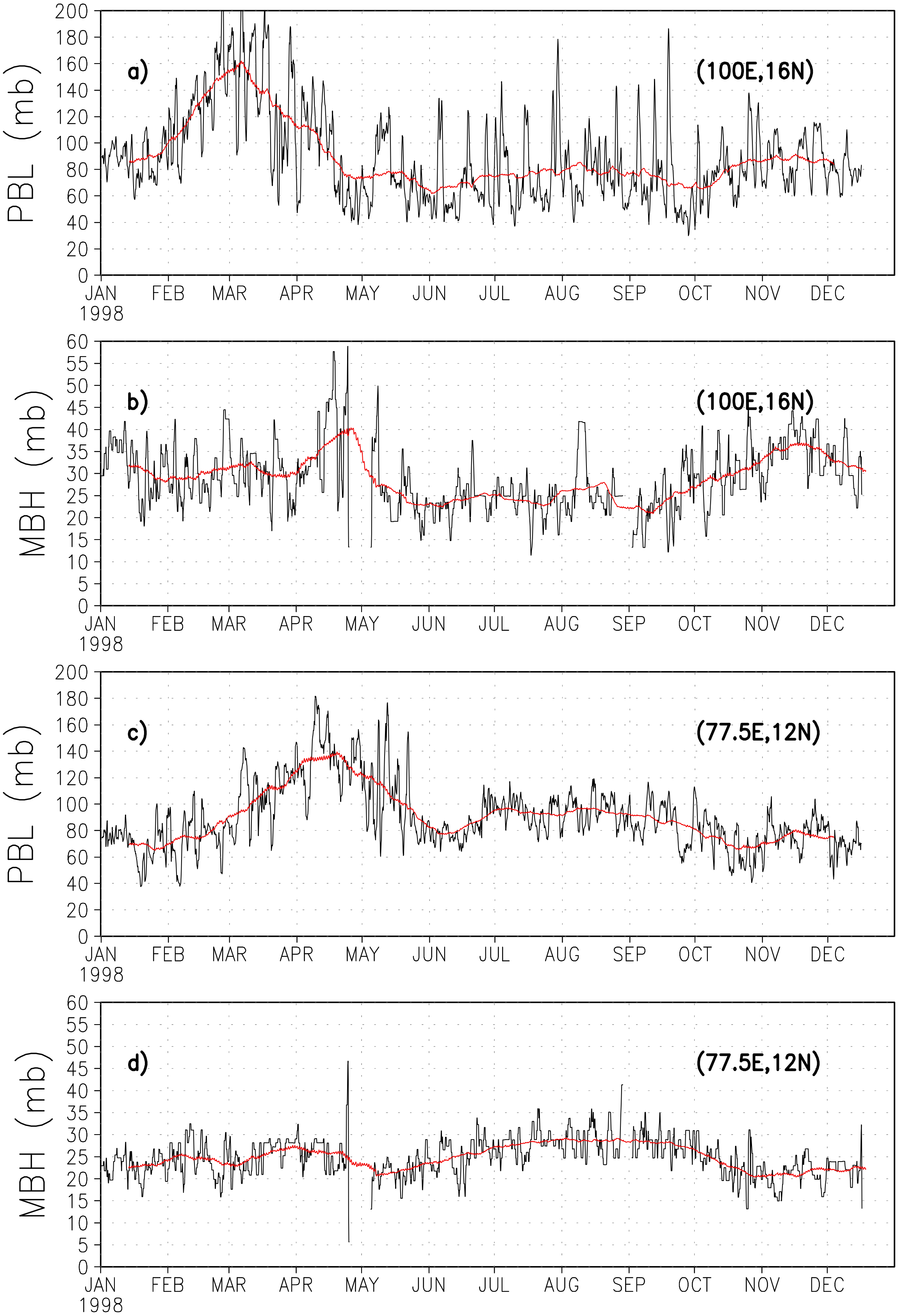

Figure 9: Time series of MBH and PBL height in mb for (100E,16N), panels a) and b), respectively, and for (77.5E,12N) in panels c) and d), respectively. Each panel contains 1-day and 30-day running means.

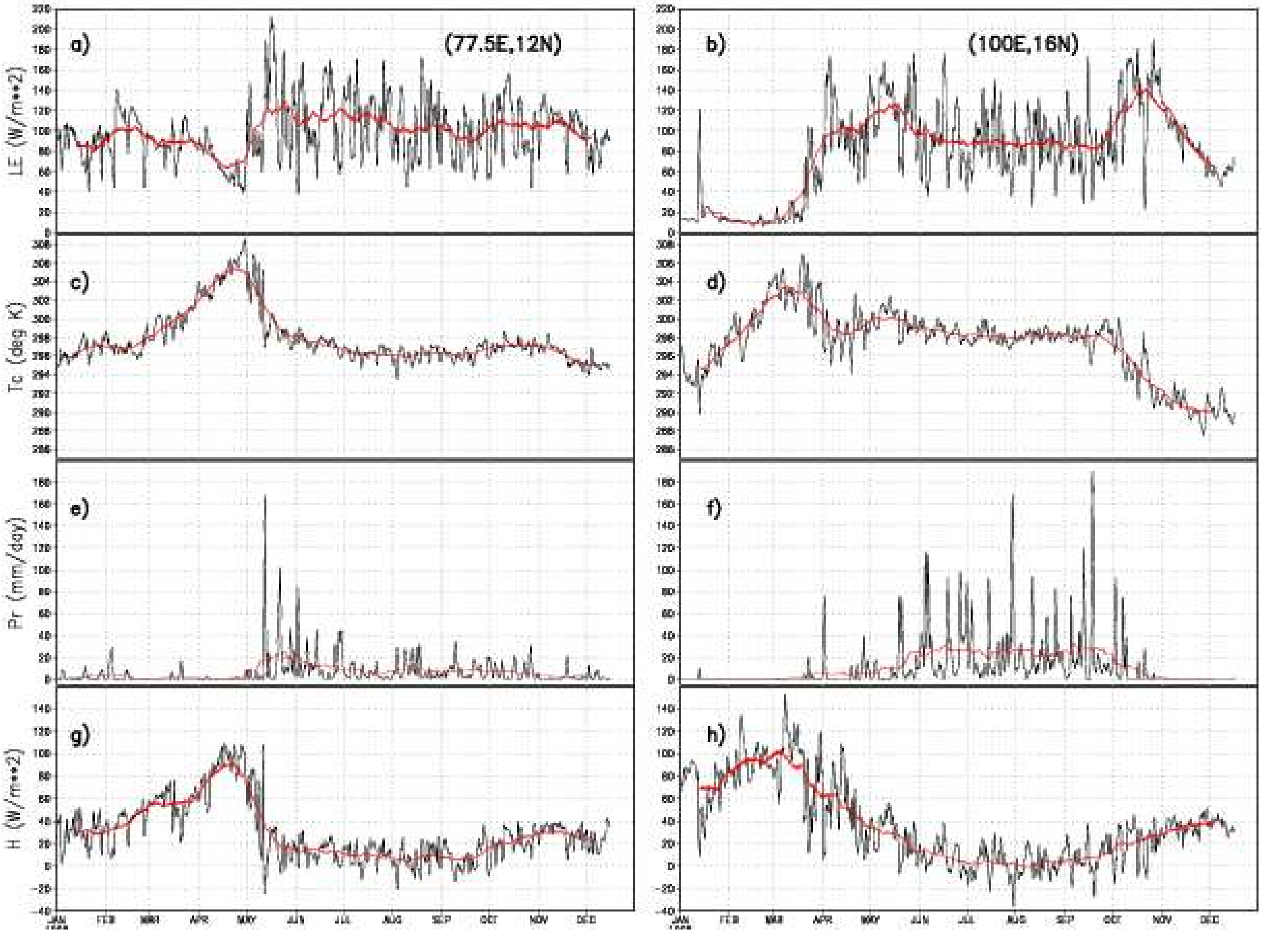

Figure 10: Time series of meteorological fields for (77.5E,12N) and (100E,16N). Panels a), c), e) and f) are latent heat flux in W m^{-2}, canopy temperature in °K, precipitation in mm day^{-1} and sensible heat flux in W m^{-2} for the point (77.5E,12N), respectively. Panels b), d), f) and h) are the corresponding plots for (100E,16N). Each panel contains 1-day and 30-day running means.